



**Detecting quantum critical points at finite temperature via quantum teleportation**G. A. P. Ribeiro  and Gustavo Rigolin \**Departamento de Física, Universidade Federal de São Carlos, 13565-905 São Carlos, SP, Brazil*

(Received 13 February 2023; revised 10 April 2023; accepted 16 May 2023; published 25 May 2023)

We show that the quantum teleportation protocol is a powerful tool to study quantum phase transitions at finite temperatures. We consider a pair of spins from an infinite spin-1/2 chain ( $XXZ$  model) in equilibrium with a reservoir at temperature  $T$  as the resource used by Alice and Bob to implement the teleportation protocol. We show that the efficiency of this pair of spins to teleport a qubit is drastically affected after we cross a quantum critical point (QCP), even for high values of  $T$ . Also, we show that the present tool is as sharp as quantum discord (QD) to spotlight a QCP, where QD is the best finite  $T$  QCP detector known to date. Contrary to QD, however, we show that the present tool is easier to compute theoretically and has a direct experimental and operational meaning.

DOI: [10.1103/PhysRevA.107.052420](https://doi.org/10.1103/PhysRevA.107.052420)**I. INTRODUCTION**

A quantum phase transition (QPT) is the abrupt change in the physical properties of a many-body system that occurs at the absolute zero temperature ( $T = 0$ ) while we change its Hamiltonian  $H$  [1]. At  $T = 0$ , the system is completely described by its ground state, a function of  $H$ . If we slowly modify  $H$ , we may reach a quantum critical point (QCP) in the parameter space where the macroscopic properties of the system abruptly change. This “change of phase” is driven solely by quantum fluctuations and is almost always characterized by a fundamental symmetry change in the system’s ground state and the emergence of an order parameter. For a magnetic system, for instance, the order parameter is the net magnetization, which becomes non-null after the system enters the ferromagnetic phase.

The physical principle behind the quantum fluctuations is the Heisenberg uncertainty principle. There is no role for thermal fluctuations in a QPT since we are in principle at  $T = 0$ , and to drive the system from one phase to another we usually change a single quantity (tuning parameter) of  $H$ . Examples of tuning parameters are the coupling constants or external fields acting on the system. The superfluid–Mott-insulator transition [2], the superconductor-insulator transition [3], and the ferromagnetic-paramagnetic transition in some metals [4] are paradigmatic examples of QPTs.

Many useful theoretical tools to investigate QPTs assume that we are exactly at  $T = 0$ . For a spin chain, the QCPs are obtained by studying the behavior of its magnetization, bipartite [5] and multipartite [6] entanglement, and more general quantum correlations [7,8] as functions of the tuning parameter. The extremal values of these quantities or discontinuities in their first- and second-order derivatives are important indicators of a QPT. However, from an experimental point of view, the  $T = 0$  condition is unattainable due to the

third law of thermodynamics, and any small deviation from  $T = 0$  brings to the table thermal fluctuations that excite the system beyond the ground state, limiting severely our ability to properly detect a genuine QCP. A remarkable example of this limitation is the inability of the entanglement of formation (EOF) [9] and the magnetic susceptibility to detect a QPT in spin chains for  $T > 0$ . For very small values of  $T$ , the former is already zero before and after the QCPs, and the latter is a smooth function of the tuning parameter with no indication of QPTs when we cross the QCPs [10,11].

In Ref. [11], however, we showed that in the thermodynamic limit (infinite chains), thermal quantum discord (TQD) [12] is a key theoretical tool that bridges the gap between the  $T = 0$  predictions of QPTs and the finite  $T$  experiments. For several classes of spin chains, we showed that TQD detects QCPs for relatively high values of  $T$ , while at this same  $T$  the EOF is already zero and other thermodynamic quantities, including the magnetic susceptibility, are not able to correctly identify the QCP or are less efficient than TQD to properly identify it.

Notwithstanding its tremendous success to detect a QCP at finite  $T$  [11], the quantum discord (QD) [13,14] has two handicaps. First, the optimization problem that one needs to solve to obtain the QD is nondeterministic polynomial-time complete (NP-complete) [15]. This means that the computation of QD is an intractable problem as we increase the size of the Hilbert space of the system under investigation. It is thus very difficult to extend the analysis of spin-1/2 chains to higher spin chains [16]. Second, QD does not have an operational meaning. There is no direct experimental procedure whose outcome is the QD. We need first to obtain the system’s density matrix and then use it to compute the QD.

In this manuscript, we present a tool that possesses all the outstanding features of TQD in detecting QCPs at finite  $T$  and, on top of that, does not have its two aforementioned handicaps. The present tool is based on the quantum teleportation protocol [17], where a pair of qubits in a spin chain is employed as the quantum resource needed to implement

\*rigolin@ufscar.br

the quantum teleportation protocol [18,19]. In Ref. [19], for two-spin systems in equilibrium with a thermal reservoir at temperature  $T$ , it was shown that the fidelity of the teleported state changes abruptly when we cross a QCP. Here we extend the results of Ref. [19] to more general settings, to more QCPs, and most importantly, we work in the thermodynamic limit.

## II. THE XXZ MODEL

The spin-1/2 chain we study here in the thermodynamic limit ( $L \rightarrow \infty$ ) is given by the following Hamiltonian ( $\hbar = 1$ ):

$$H = \sum_{j=1}^L (\sigma_j^x \sigma_{j+1}^x + \sigma_j^y \sigma_{j+1}^y + \Delta \sigma_j^z \sigma_{j+1}^z). \quad (1)$$

We employ periodic boundary conditions, and  $\sigma_j^x, \sigma_j^y, \sigma_j^z$  are the standard Pauli matrices associated with the qubit  $j$ . The anisotropy  $\Delta$  is our tuning parameter, and at  $T = 0$  this model has two QCPs [20]. At  $\Delta = -1$  we have a first-order transition. The ground state changes from a ferromagnetic phase ( $\Delta < -1$ ) to the critical antiferromagnetic one ( $-1 < \Delta < 1$ ). At  $\Delta = 1$ , we have a continuous phase transition with the system becoming an Ising-like antiferromagnet when  $\Delta > 1$ .

In thermal equilibrium with a reservoir at temperature  $T$ , the density matrix describing this chain is  $\varrho = e^{-H/kT}/Z$ , with  $Z = \text{Tr}[e^{-H/kT}]$  the partition function and  $k$  Boltzmann's constant. Tracing out from  $\varrho$  all but two nearest neighbors gives the two-spin state [11]

$$\rho_{j,j+1} = \begin{pmatrix} \frac{1 + \langle \sigma_j^z \sigma_{j+1}^z \rangle}{4} & 0 & 0 & 0 \\ 0 & \frac{1 - \langle \sigma_j^z \sigma_{j+1}^z \rangle}{4} & \frac{\langle \sigma_j^x \sigma_{j+1}^x \rangle}{2} & 0 \\ 0 & \frac{\langle \sigma_j^x \sigma_{j+1}^x \rangle}{2} & \frac{1 - \langle \sigma_j^z \sigma_{j+1}^z \rangle}{4} & 0 \\ 0 & 0 & 0 & \frac{1 + \langle \sigma_j^z \sigma_{j+1}^z \rangle}{4} \end{pmatrix}. \quad (2)$$

The computation of the two-point correlation functions  $\langle \sigma_j^\alpha \sigma_{j+1}^\alpha \rangle = \text{Tr}[\sigma_j^\alpha \sigma_{j+1}^\alpha \varrho]$ , with  $\alpha = x, z$ , in the thermodynamic limit for arbitrary  $T$  and  $\Delta$  was done in Refs. [21–24] and reviewed in Ref. [11] (see Appendix A).

## III. THE TELEPORTATION PROTOCOL

Equation (2) describes the resource through which we implement the teleportation protocol. Setting  $j = 2$ , the two-qubit state at sites 2 and 3 (see Fig. 1) is what one usually calls the state shared by Alice and Bob at the beginning of the teleportation protocol. The qubit to be teleported (spin 1 in Fig. 1) is external to the chain and can be prepared in any normalized pure state ( $0 \leq r \leq 1$  and  $0 \leq \gamma < 2\pi$ ),

$$|\psi\rangle = r|0\rangle + \sqrt{1-r^2}e^{i\gamma}|1\rangle. \quad (3)$$

The initial state describing the three qubits before the beginning of the teleportation protocol is

$$\rho = \rho_1 \otimes \rho_{23}, \quad (4)$$

where  $\rho_1 = |\psi\rangle\langle\psi|$ , and  $\rho_{23}$  is given by Eq. (2). At the end of a given run of the protocol, i.e., after the four steps described

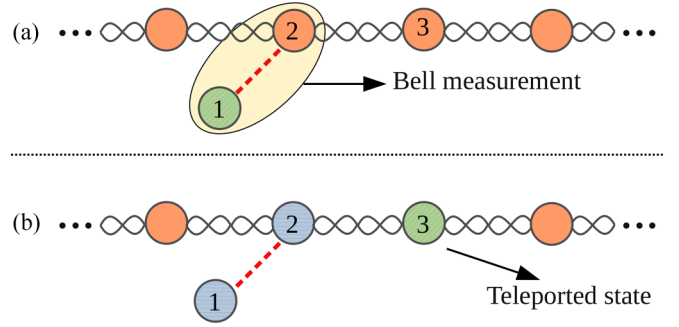


FIG. 1. The teleportation protocol works as follows [17]. (a) First, one prepares the entangled resource (spins 2 and 3) to be used to teleport the input (spin 1). Second, a Bell measurement (BM) is made by Alice on spins 1 and 2. (b) Third, Alice informs Bob of her BM result using a classical communication channel. Fourth, Bob applies a unitary operation on spin 3, which depends on Alice's BM result, to finish the protocol.

in Fig. 1, Bob's qubit (spin 3) is given by [19]

$$\rho_{B_j} = \{U_j \text{Tr}_{12}[P_j \rho P_j] U_j^\dagger\} / Q_j(|\psi\rangle), \quad (5)$$

where  $\text{Tr}_{12}$  is the partial trace on Alice's qubits (spins 1 and 2). In Eq. (5),  $j$  denotes the BM result obtained by Alice, namely  $j = \Psi^-, \Psi^+, \Phi^-, \Phi^+$ , and  $P_j$  denotes the four projectors describing her BMs,  $P_{\Psi^\pm} = |\Psi^\pm\rangle\langle\Psi^\pm|$  and  $P_{\Phi^\pm} = |\Phi^\pm\rangle\langle\Phi^\pm|$ , where the Bell states are  $|\Psi^\mp\rangle = (|01\rangle \mp |10\rangle)/\sqrt{2}$  and  $|\Phi^\mp\rangle = (|00\rangle \mp |11\rangle)/\sqrt{2}$ .

Alice's probability to measure Bell state  $j$  is

$$Q_j(|\psi\rangle) = \text{Tr}[P_j \rho], \quad (6)$$

and the unitary operation that Bob must implement on his qubit after being informed of Alice's BM result is  $U_j$ .

The unitary operation  $U_j$  that Bob must implement on his qubit at the end of the protocol is also dependent on the entangled resource shared by Alice and Bob. In its standard formulation [17], where they share a maximally entangled pure state (Bell state), we have

$$S_{\Phi^+} = \{U_{\Phi^+}, U_{\Phi^-}, U_{\Psi^+}, U_{\Psi^-}\} = \{\mathbb{1}, \sigma^z, \sigma^x, \sigma^z \sigma^x\} \quad (7)$$

if the shared Bell state is  $|\Phi^+\rangle$ , with  $\mathbb{1}$  being the identity matrix, and for  $|\Phi^-\rangle$  and  $|\Psi^\pm\rangle$ , we have, respectively,

$$S_{\Phi^-} = \{U_{\Phi^+}, U_{\Phi^-}, U_{\Psi^+}, U_{\Psi^-}\} = \{\sigma^z, \mathbb{1}, \sigma^z \sigma^x, \sigma^x\}, \quad (8)$$

$$S_{\Psi^+} = \{U_{\Phi^+}, U_{\Phi^-}, U_{\Psi^+}, U_{\Psi^-}\} = \{\sigma^x, \sigma^z \sigma^x, \mathbb{1}, \sigma^z\}, \quad (9)$$

$$S_{\Psi^-} = \{U_{\Phi^+}, U_{\Phi^-}, U_{\Psi^+}, U_{\Psi^-}\} = \{\sigma^z \sigma^x, \sigma^x, \sigma^z, \mathbb{1}\}. \quad (10)$$

In the present case, the state  $\rho_{23}$  shared by Alice and Bob is not pure and is approximately described by one Bell state in one phase and by a different one in another phase. Therefore, when characterizing the QCPs of a spin chain, we will work with the four possible sets of unitary operations above. As we will see, this approach is crucial to obtain the most efficient QCP detector based on the teleportation protocol.

To quantify the similarity between the teleported state, i.e., Bob's qubit at the end of the protocol (spin 3), with the input state teleported by Alice (spin 1), we use the fidelity [25]. For

a pure input state, we have

$$F_j(|\psi\rangle, S_k) = \langle \psi | \rho_{B_j} | \psi \rangle, \quad (11)$$

where  $|\psi\rangle$  is given by Eq. (4) and  $\rho_{B_j}$  by Eq. (5). If the teleported state is exactly the input state,  $F_j = 1$ , and  $F_j = 0$  if the output is orthogonal to the input. Note that in general  $F_j$  depends on the input state, the entangled resource shared by Alice and Bob, and on the set of unitary corrections  $S_k$  chosen by Bob. Here the entangled resource is fixed and is given by Eq. (2), while we can freely choose  $|\psi\rangle$  and  $S_k$ , with  $k = \Psi^\mp, \Phi^\mp$ .

For a fixed input state, after several runs of the protocol the mean fidelity (efficiency) is [26,27]

$$\bar{F}(|\psi\rangle, S_k) = \sum_{j=\Psi^\mp, \Phi^\mp} Q_j(|\psi\rangle) F_j(|\psi\rangle, S_k). \quad (12)$$

If we want an input state-independent measure of the efficiency of the teleportation protocol, we can average over all states on the Bloch sphere. This is equivalent to considering in Eq. (3)  $r^2$  and  $\gamma$  as independent continuous random variables over their allowed values [26,27]. Formally, this input state-independent mean fidelity, average fidelity for short, can be written as [19,26–28]

$$\langle \bar{F}(S_k) \rangle = \int_{\Omega} \bar{F}(|\psi\rangle, S_k) \mathcal{P}(|\psi\rangle) d|\psi\rangle, \quad (13)$$

where we integrate over the sample space  $\Omega$  comprised of all qubits on the Bloch sphere, and  $\mathcal{P}(|\psi\rangle)$  is the corresponding uniform probability distribution over  $\Omega$ .

Before we specialize to the  $XXZ$  model, two remarks are in order. First, from an experimental point of view, the present analysis is meaningful when the time needed to execute the four steps of the teleportation protocol is shorter than the time needed by the system to get back to equilibrium with the thermal reservoir. The rate at which we implement all four steps of the protocol should be greater than the thermal relaxation rate of the system. We should determine the state of the qubit teleported to Bob before it thermalizes once again.<sup>1</sup> Nevertheless, the experimental procedure needed to teleport a qubit and measure Bob's state is clear and can in principle be implemented using state-of-the-art techniques [29–35]. Knowing Bob's state at the end of the teleportation protocol for a representative sample of input states lying on the Bloch sphere is all we need to determine Eqs. (12) and (13). This should be contrasted with the determination of the EOF or the QD of a pair of spins. There is no direct experimental procedure to measure those quantities for arbitrary mixed states. To compute those quantities, we must have access to the complete density matrix describing the two qubits (spins 2 and 3) [9,13,14]. For the  $XXZ$  model, for instance, we must have the complete knowledge of Eq. (2). On the other hand, to experimentally determine Bob's state at the end of

the teleportation protocol, we just need the single qubit density matrix describing it. We only need to measure one-point correlation functions instead of the two-point ones needed for the computation of the EOF or the QD.

Second, the choice for the fidelity to assess the similarity between Alice's input state and Bob's output state at the end of the teleportation protocol is not mandatory. We could have used any other measure to quantify the similarity between those two states. As such, the present proposal to detect QCPs should not be confused with the ones based on the computation of the fidelity or the fidelity susceptibility between the system's whole ground state before and after the QCP [36–41]. Our proposal is conceptually different from the ones studied in the aforementioned references. In our proposal, the teleportation protocol plays an active and key role in its implementation; no mention or use of the quantum teleportation protocol are present in Refs. [36–41]. Also, to fully implement the ideas of Refs. [36–41] without any approximation, one needs to know the whole ground state of the chain before and after the QCP to compute the fidelity between those states. In our approach, from a theoretical point of view, we only need up to two-point correlation functions to compute the efficiency of the teleportation protocol. There is no need to know the whole ground state. Indeed, the determination of the whole ground state of the system requires much more information: one should in principle have access to all  $n$ -point correlation functions, where  $n = 1, 2, 3, \dots, L$ , with  $L$  being the size of the spin chain. This clearly sets apart our approach (and the ones based on quantum discord and entanglement of formation between two spins) from those of Refs. [36–41]. Here we have a local approach, i.e., we only need up to two-point correlation functions to implement our idea. In Refs. [36–41] we have a global approach, i.e., we need the whole ground state to make progress. This is another feature that clearly sets apart both strategies. It also means that the present method allows us to properly detect QCPs using local finite- $T$  data alone.

#### IV. RESULTS

If we insert Eq. (4) into (6), we get  $Q_j(|\psi\rangle) = 1/4$  for all  $j$ . This means that Alice obtains with equal chances any one of the four Bell states after the BM on qubits 1 and 2. Note that the probabilities  $Q_j$  are all independent of the input state (qubit 1). This is a particular feature of the  $XXZ$  model without external fields, and it can be traced back to the specific form of Eq. (2).

Another feature of the present model is that Eq. (11) leads to  $F_{\Psi^\mp}(|\psi\rangle, S_k) = F_{\Phi^\mp}(|\psi\rangle, S_k)$ . In other words,  $F_j$  is independent of  $j$ , i.e., independent of the outcome of Alice's BM. Therefore, for the present model, Eq. (12) can be written as  $\bar{F}(|\psi\rangle, S_k) = F_j(|\psi\rangle, S_k)$ , for any  $j$ .

If we maximize over all pure states and over  $S_k$ , we get for the overall maximum fidelity (see Appendix B)

$$\bar{\mathcal{F}} = \max_{\{|\psi\rangle, S_k\}} \bar{F}(|\psi\rangle, S_k) = \max \left[ \frac{1 + |\langle \sigma_2^z \sigma_3^z \rangle|}{2}, \frac{1 + |\langle \sigma_2^x \sigma_3^x \rangle|}{2} \right]. \quad (14)$$

<sup>1</sup>The determination of the relaxation time is a tricky and nontrivial problem, the calculation of which is beyond the scope of the present work. The relaxation time depends not only on the internal dynamics of the spin chain (its Hamiltonian) but also on how it interacts with the heat bath.

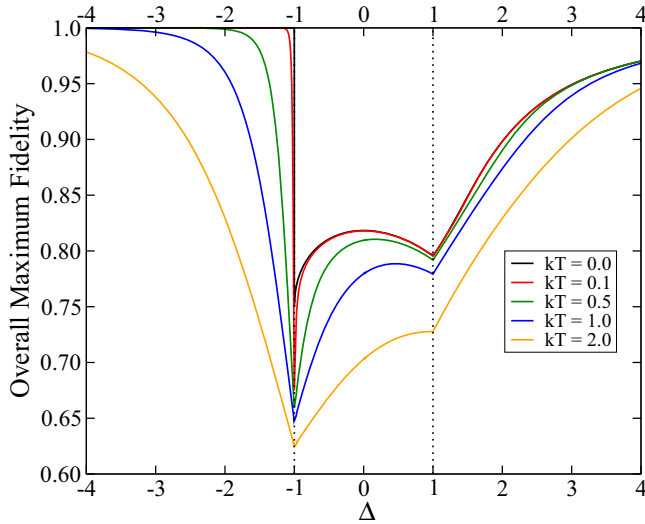


FIG. 2.  $\overline{\mathcal{F}}$ , Eq. (14), as a function of the anisotropy  $\Delta$  that characterizes the XXZ model [Eq. (1)]. Both QCPs are detected at  $T = 0$  and  $T > 0$  by a discontinuity in the first derivative of  $\overline{\mathcal{F}}$  with respect to  $\Delta$ . In the curves above, temperature increases from top to bottom. Here and in all other figures, all quantities are dimensionless.

The extrema of Eq. (12) occur for the input states  $|\psi\rangle = |1\rangle$  and  $|\psi\rangle = (|0\rangle + e^{i\gamma}|1\rangle)/\sqrt{2}$  (see Appendix B). Which state leads to the maximum (or minimum) fidelity depends on the phase of the spin chain and on the sign of the two-point correlation functions.

In Fig. 2, we plot  $\overline{\mathcal{F}}$  as a function of  $\Delta$  for several values of  $T$ . It is clear from Fig. 2 that  $\overline{\mathcal{F}}$  detects both QCPs when  $T = 0$  and for  $T > 0$ . It is worth mentioning that for  $kT \gtrsim 0.1$  the EOF is already zero before, at, and after the QCP  $\Delta = -1$  [11]. The cusplike behavior of  $\overline{\mathcal{F}}$  at the two QCPs is similar to that observed for the TQD [11]. The discontinuity of the first derivative of  $\overline{\mathcal{F}}$  with respect to the tuning parameter  $\Delta$  is related to the fact that at the two QCPs, the roles of  $|\langle\sigma_2^x\sigma_3^x\rangle|$  and  $|\langle\sigma_2^z\sigma_3^z\rangle|$  are exchanged. For instance, in one phase the maximum of  $\overline{\mathcal{F}}$  is a function of  $|\langle\sigma_2^z\sigma_3^z\rangle|$ , while at the other phase it is a function of  $|\langle\sigma_2^x\sigma_3^x\rangle|$ .

If we now employ Eq. (13), maximized over the sets  $S_k$  of unitary operations available to Bob, we get (see Appendix B)

$$\begin{aligned} \langle\overline{\mathcal{F}}\rangle &= \max_{\{S_k\}} \langle\overline{F}(S_k)\rangle \\ &= \max \left[ \frac{3 + 2|\langle\sigma_2^x\sigma_3^x\rangle| - \langle\sigma_2^z\sigma_3^z\rangle}{6}, \frac{3 + \langle\sigma_2^z\sigma_3^z\rangle}{6} \right]. \end{aligned} \quad (15)$$

Looking at Fig. 3, we realize that the QCP located at  $\Delta = -1$ , associated with a first-order QPT, is clearly detected for  $T = 0$  and  $T > 0$ . The cusplike behavior of  $\langle\overline{\mathcal{F}}\rangle$  at  $\Delta = -1$  for  $T = 0$  and  $T > 0$  clearly indicates a QPT. The other QCP,  $\Delta = 1$ , related to a continuous QPT is detected at  $T = 0$  by noting that  $\langle\overline{\mathcal{F}}\rangle$  has its global maximum exactly at  $\Delta = 1$ . For finite  $T$  this maximum is displaced to higher values of  $\Delta$ . Contrary to  $\overline{\mathcal{F}}$ ,  $\langle\overline{\mathcal{F}}\rangle$  does not have a cusp at  $\Delta = 1$ . However, if we work with both the maximum and minimum of  $\langle\overline{F}(S_k)\rangle$ , we can get a cusplike behavior at both QCPs (see Appendix C).

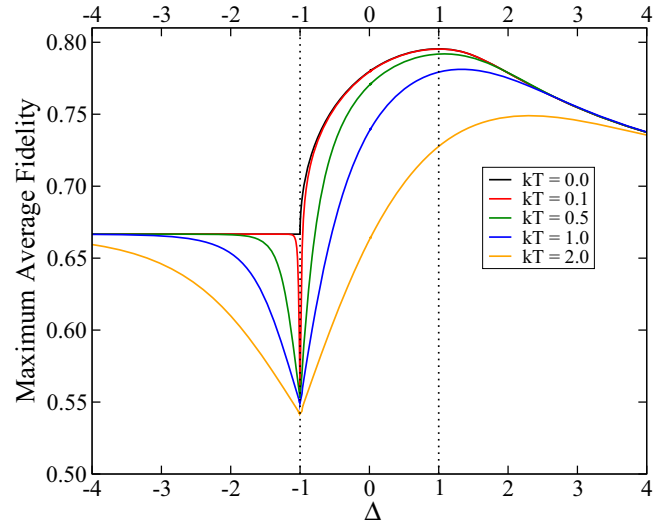


FIG. 3. Same as Fig. 2 but now we plot  $\langle\overline{\mathcal{F}}\rangle$ , Eq. (15). The QCP at  $\Delta = -1$  is detected at  $T = 0$  and  $T > 0$  by a discontinuity in the first derivative of  $\langle\overline{\mathcal{F}}\rangle$  with respect to  $\Delta$ . The other QCP is obtained at  $T = 0$  noting that  $\langle\overline{\mathcal{F}}\rangle$  is maximal at  $\Delta = 1$ . For finite  $T$ , the maximum is displaced to greater values of  $\Delta$ . For  $kT \lesssim 1.0$  these maxima lie close together, and by extrapolating to  $kT \rightarrow 0$  we can infer this QCP by working with finite- $T$  data. In the curves above, temperature increases from top to bottom.

The usefulness of  $\overline{\mathcal{F}}$  and  $\langle\overline{\mathcal{F}}\rangle$  to pinpoint a QCP is not restricted to the XXZ model. They are as good as TQD [11] to detect for  $T > 0$  the QCP of the XXX model (see Appendix D). It remains an open problem to check if the ideas presented here apply to the detection of pseudotransitions [42,43].

## V. DISCUSSION AND CONCLUSION

As already highlighted above, the operational and experimental interpretation of the fidelities is very clear and straightforward. For the XXZ and XXX model with no fields, whose two-qubit density matrix is given by Eq. (2), the experimental demands to implement the present proposal are further reduced. Since for those models  $\overline{F}(|\psi\rangle, S_k) = F_j(|\psi\rangle, S_k)$ , we do not need to implement any unitary correction  $U_j$  on the teleported qubit to obtain the fidelities. We just need to separate the data into four sets, each one corresponding to the four possible outcomes of Alice's BMs. In this way, we automatically get the mean fidelities  $\overline{F}(|\psi\rangle, S_k)$  related to each one of the four sets  $S_k$ . Teleporting a representative sample of qubits covering the Bloch sphere, we obtain  $\overline{\mathcal{F}}$  picking from this sample of teleported states the case yielding the greatest fidelity and, averaging over all cases, we get  $\langle\overline{\mathcal{F}}\rangle$ . To fully execute the teleportation protocol, we also need to be able to implement the BMs on qubits 1 and 2. The BMs can be made by applying a controlled-not (CNOT) operation on those qubits [29–35] followed by a Hadamard operation on the control qubit and a measurement of those spins in the computational basis [44]. For instance, if after the previous prescription we see spins 1 and 2 pointing up ( $|00\rangle$ ) or down ( $|11\rangle$ ), it means

that we have projected them onto the Bell state  $|\Phi^+\rangle$  or  $|\Psi^-\rangle$  [44].

From the theoretical point of view, and similarly to EOF and QD, we need the two-qubit density matrix, Eq. (2), to compute the fidelity. In a more general scenario (higher spins), we need the bipartite density matrix describing two  $N$ -dimensional systems. However, and contrary to EOF and QD, the computational resources needed to compute the fidelity are less demanding. To compute the maximum average fidelity, Eq. (15), we just need to repeat for each one of the four sets of unitary operations  $S_k$  the calculation of the average fidelity, Eq. (13). The calculation of the latter is a very simple matter and can be efficiently scaled to an  $N$ -dimensional input state  $|\psi\rangle$  [27]. To calculate the overall maximum fidelity, Eq. (14), we have to repeat the maximization of Eq. (12) over all input states  $|\psi\rangle$  four times (for each one of the four sets of unitary operations  $S_k$ ). Since an  $N$ -dimensional pure state is describe by  $2N - 2$  independent parameters [45], we will face an optimization problem involving  $2N - 2$  free variables. For high values of  $N$  this is not a simple problem, but it is less demanding than solving the corresponding optimization problem to determine the QD, where we must minimize the conditional entropy over all sets of generalized measurements (POVMs) [13–15]. These POVMs are  $N \times N$  matrices, and the number of free parameters increases faster than linearly with  $N$  [15]. The intuitive reason for this difference in computational demand rests on the fact that for the overall maximum fidelity we optimize over a single pure state, while for QD the optimization problem is equivalent to the complexity of determining the EOF, whose optimization is done over all ensembles of pure states into which  $\rho_{23}$  can be decomposed [15].

Summing up, we have presented two teleportation-based theoretical tools to detect QCPs at finite  $T$  equivalent to TQD, the most reliable QCP detector for finite  $T$  known to date. Both tools work without the knowledge of the order parameter associated with the QPT. The tools presented here have two features that set them apart from TQD and other quantum information theory based QCP detectors. First, they have a straightforward experimental interpretation and can in principle be directly measured in the laboratory. Second, from a theoretical point of view we need fewer computational resources to calculate them when compared to TQD, with one of these tools, the average fidelity, easily scalable to an  $N$ -dimensional spin system.

#### ACKNOWLEDGMENTS

G.R. thanks the Brazilian agency CNPq (National Council for Scientific and Technological Development) for funding, and CNPq/FAPERJ (State of Rio de Janeiro Research Foundation) for financial support through the National Institute of Science and Technology for Quantum Information.

#### APPENDIX A: TWO-POINT CORRELATION FUNCTIONS

The XXZ model we studied is given by Eq. (1) of the main text. In thermal equilibrium with a reservoir at temperature  $T$ , the non-null two-point correlation functions are  $\langle \sigma_j^x \sigma_{j+1}^x \rangle = \langle \sigma_j^y \sigma_{j+1}^y \rangle$  and  $\langle \sigma_j^z \sigma_{j+1}^z \rangle$ . The techniques to solve

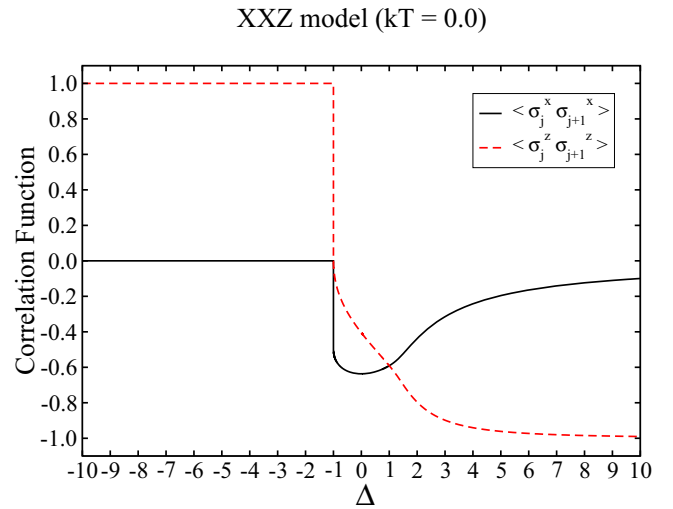


FIG. 4. Two-point correlation functions in the thermodynamic limit at  $T = 0$  as a function of the tuning parameter  $\Delta$ .

this problem in the thermodynamic limit (infinite chain) were developed in Refs. [21–24], and they were carefully reviewed, adapted, and implemented for the present context in Ref. [11].

At the absolute zero temperature, the two-point correlation functions are given by Figs. 4 and 5 [11].

For finite  $T$ , the behavior of the two-point correlation functions is given by Figs. 6 and 7 [11].

Note that at the quantum critical points (QCPs), the two-point correlation function having the greatest magnitude changes. This is particularly clear for low values of  $kT$ . Before  $\Delta = -1$ ,  $|\langle \sigma_j^z \sigma_{j+1}^z \rangle| > |\langle \sigma_j^x \sigma_{j+1}^x \rangle|$  while after  $\Delta = -1$ ,  $|\langle \sigma_j^x \sigma_{j+1}^x \rangle| > |\langle \sigma_j^z \sigma_{j+1}^z \rangle|$ . This behavior is also seen before and after the other QCP at  $\Delta = 1$  and it is the reason for the cusplike behavior of the overall maximum fidelity  $\overline{\mathcal{F}}$  at both QCPs (see the main text).

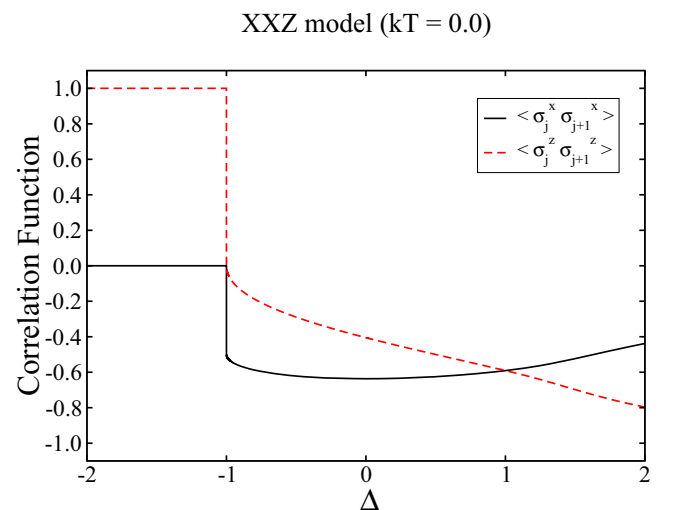


FIG. 5. Two-point correlation functions in the thermodynamic limit at  $T = 0$  as a function of the tuning parameter  $\Delta$ .

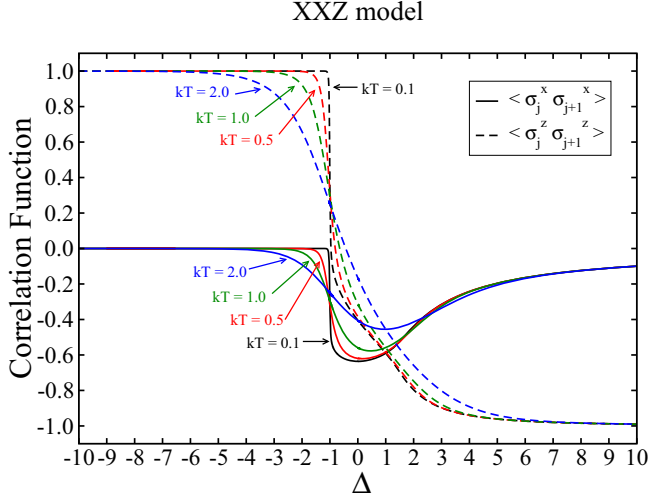


FIG. 6. Two-point correlation functions in the thermodynamic limit for  $T > 0$  as a function of the tuning parameter  $\Delta$ .

### APPENDIX B: OBTAINING $\bar{\mathcal{F}}$ AND $\langle \bar{\mathcal{F}} \rangle$

In the XXZ model, we have  $Q_j(|\psi\rangle) = 1/4$  and  $F_j(|\psi\rangle, S_k) = F_{j'}(|\psi\rangle, S_k)$  for any  $j, j' = \Psi^\mp, \Phi^\mp$ . Thus, a direct calculation using Eqs. (3)–(5) and (11) of the main text allows us to write Eq. (12) of the main text as follows:

$$\bar{F}(|\psi\rangle, S_{\Psi^-}) = f(r, -xx, zz), \quad (\text{B1})$$

$$\bar{F}(|\psi\rangle, S_{\Psi^+}) = f(r, xx, zz), \quad (\text{B2})$$

$$\bar{F}(|\psi\rangle, S_{\Phi^-}) = g(r, \gamma, -xx, zz), \quad (\text{B3})$$

$$\bar{F}(|\psi\rangle, S_{\Phi^+}) = g(r, \gamma, xx, zz), \quad (\text{B4})$$

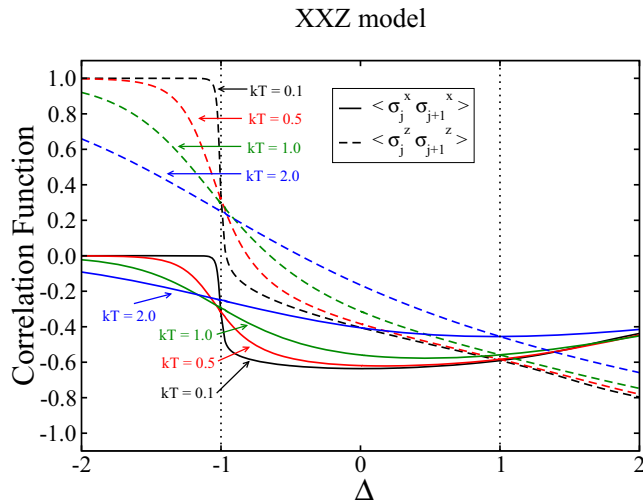


FIG. 7. Two-point correlation functions in the thermodynamic limit for  $T > 0$  as a function of the tuning parameter  $\Delta$ .

where

$$f(r, xx, zz) = [1 + 4r^2(1 - r^2)(xx + zz) - zz]/2, \quad (\text{B5})$$

$$g(r, \gamma, xx, zz) = [1 + (1 - 2r^2)^2 zz + 4r^2(1 - r^2)xx \cos(2\gamma)]/2, \quad (\text{B6})$$

$$xx = \langle \sigma_j^x \sigma_{j+1}^x \rangle, \quad (\text{B7})$$

$$zz = \langle \sigma_j^z \sigma_{j+1}^z \rangle. \quad (\text{B8})$$

Computing the extrema of  $f(r, xx, zz)$ , i.e., solving

$$\frac{\partial f}{\partial r} = 0, \quad (\text{B9})$$

we immediately get for  $r \geq 0$

$$r = 0, 1/\sqrt{2}. \quad (\text{B10})$$

This means, according to Eq. (3) of the main text, that the states leading to the extrema of  $\bar{F}(|\psi\rangle, S_{\Psi^\mp})$  are, up to an overall phase, either  $|1\rangle$  or  $(|0\rangle + e^{i\gamma}|1\rangle)/\sqrt{2}$ .

If we now compute the extrema of  $g(r, \gamma, xx, zz)$ , i.e., if we solve

$$\frac{\partial g}{\partial r} = 0, \quad (\text{B11})$$

$$\frac{\partial g}{\partial \gamma} = 0, \quad (\text{B12})$$

we obtain

$$(r; \gamma) = (0; 0 \leq \gamma < 2\pi), \quad (\text{B13})$$

$$(r; \gamma) = (1/\sqrt{2}; 0, \pi/2, \pi, 3\pi/2). \quad (\text{B14})$$

This implies that the input states leading to the extrema of  $\bar{F}(|\psi\rangle, S_{\Phi^\mp})$  are, up to an overall phase,  $|1\rangle$ ,  $(|0\rangle \pm |1\rangle)/\sqrt{2}$ , and  $(|0\rangle \pm i|1\rangle)/\sqrt{2}$ .

Inserting the corresponding values of  $r$  and  $\gamma$  for the extrema of the fidelity, we get

$$\bar{F}(r = 0, S_{\Psi^\mp}) = (1 - zz)/2, \quad (\text{B15})$$

$$\bar{F}(r = 1/\sqrt{2}, S_{\Psi^\mp}) = (1 \mp xx)/2, \quad (\text{B16})$$

$$\bar{F}(r = 0, S_{\Phi^\mp}) = (1 + zz)/2, \quad (\text{B17})$$

$$\bar{F}(r = 1/\sqrt{2}, \gamma, S_{\Phi^\mp}) = [1 \mp xx \cos(2\gamma)]/2. \quad (\text{B18})$$

Therefore, Eqs. (B15)–(B18) lead to

$$\bar{\mathcal{F}} = \max_{\{|\psi\rangle, S_k\}} \bar{F}(|\psi\rangle, S_k) = \max \left[ \frac{1 + |zz|}{2}, \frac{1 + |xx|}{2} \right], \quad (\text{B19})$$

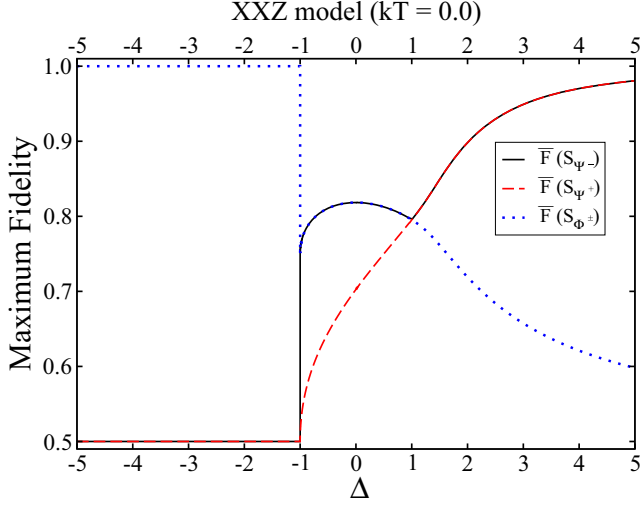
which is exactly Eq. (14) of the main text.

Moving to the calculation of  $\langle \bar{\mathcal{F}} \rangle$ , we first note that if we write the input state as

$$|\psi\rangle = a|0\rangle + b|1\rangle, \quad (\text{B20})$$

where  $|a|^2 + |b|^2 = 1$ , Eq. (13) of the main text becomes

$$\langle \bar{F}(S_{\Psi^\mp}) \rangle = [(\langle |a|^4 \rangle + \langle |b|^4 \rangle)(1 - zz) + 2\langle |ab|^2 \rangle(1 \mp 2xx + zz)]/2. \quad (\text{B21})$$


 FIG. 8.  $\overline{F}(S_k)$  as a function of  $\Delta$  at the absolute zero temperature.

If  $|a|^2$  (the probability of finding the input in the state  $|0\rangle$ ) and the relative phase between the complex numbers  $a$  and  $b$  are given by two independent continuous uniform distributions, we have [26,27]

$$\langle |a|^4 \rangle = \langle |b|^4 \rangle = 1/3, \quad \langle |ab|^2 \rangle = 1/6. \quad (\text{B22})$$

Note that we will obtain the same averages if we use the Bloch sphere representation for the input state [44],

$$|\psi\rangle = \cos(\theta/2)|0\rangle + \sin(\theta/2)e^{i\varphi}|1\rangle, \quad (\text{B23})$$

and average over the whole Bloch sphere. In this case, using the notation of Eq. (13) of the main text,  $d|\psi\rangle = dA = \sin\theta d\theta d\varphi$  is the element of area of a unit sphere written in spherical polar coordinates,  $\mathcal{P}(|\psi\rangle) = 1/(4\pi)$ ,  $0 \leq \theta \leq \pi$ , and  $0 \leq \varphi \leq 2\pi$ .

Thus, using Eq. (B22), we get for Eq. (B21)

$$\langle \overline{F}(S_{\psi^\mp}) \rangle = (3 \mp 2xx - zz)/6. \quad (\text{B24})$$

In an analogous way, we obtain

$$\langle \overline{F}(S_{\phi^\mp}) \rangle = (3 + zz)/6, \quad (\text{B25})$$

where to arrive at Eq. (B25) we also used that

$$\langle (a^*b)^2 \rangle = \langle (ab^*)^2 \rangle = 0, \quad (\text{B26})$$

with  $a^*$  ( $b^*$ ) denoting the complex conjugate of  $a$  ( $b$ ). Finally, looking at Eqs. (B24) and (B25), we get

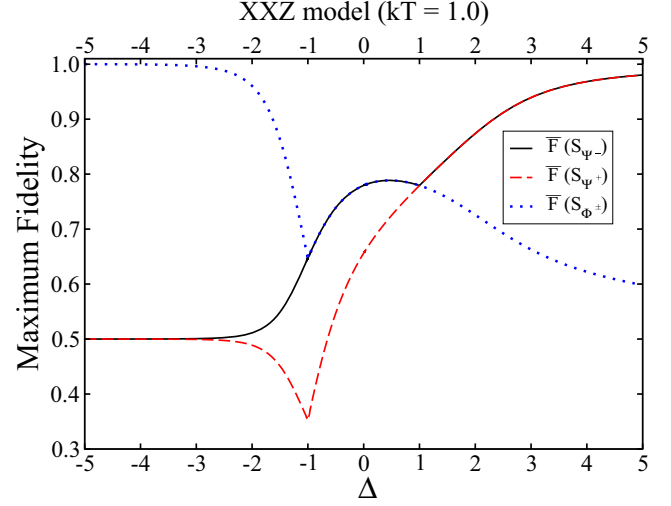
$$\begin{aligned} \langle \overline{\mathcal{F}} \rangle &= \max_{\{S_k\}} \langle \overline{F}(S_k) \rangle \\ &= \max \left[ \frac{3 + 2|xx| - zz}{6}, \frac{3 + zz}{6} \right], \end{aligned} \quad (\text{B27})$$

which is Eq. (15) of the main text.

### APPENDIX C: LOOKING DEEPER AT $\overline{\mathcal{F}}$ AND $\langle \overline{\mathcal{F}} \rangle$

To better understand the behavior of the curves shown in Fig. 2 of the main text, we will study the behavior of the following quantity:

$$\overline{F}(S_k) = \max_{\{|\psi\rangle\}} \overline{F}(|\psi\rangle, S_k). \quad (\text{C1})$$


 FIG. 9. Same as Fig. 8 but at  $kT = 1.0$ .

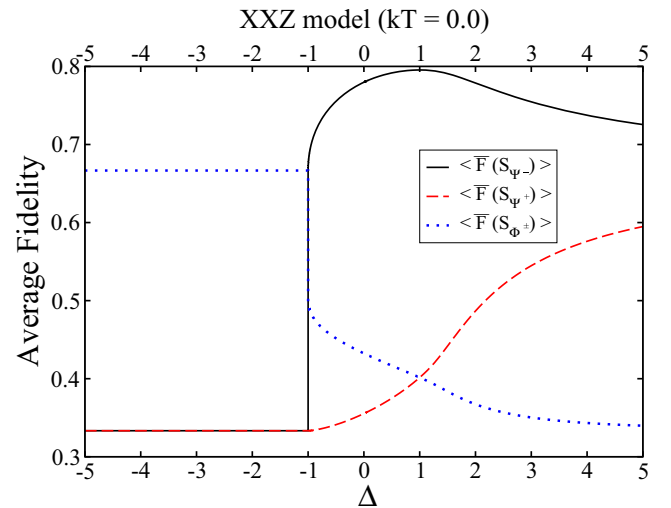
Equation (C1) is the mean fidelity, Eq. (12) of the main text, maximized over the input states only. We want to investigate the behavior of  $\overline{F}(S_k)$  for each one of the four possible values of  $k$ ,

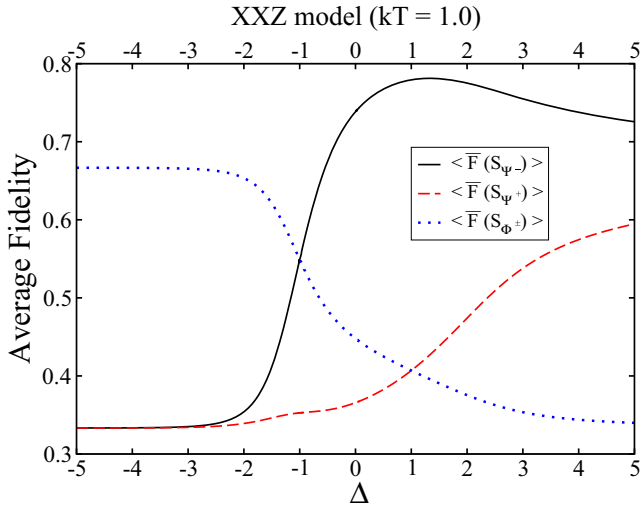
$$\overline{F}(S_{\psi^\mp}) = \max \left[ \frac{1 - zz}{2}, \frac{1 \mp xx}{2} \right], \quad (\text{C2})$$

$$\overline{F}(S_{\phi^\mp}) = \max \left[ \frac{1 + zz}{2}, \frac{1 + |xx|}{2} \right]. \quad (\text{C3})$$

Proceeding in this way, we will be able to trace back which expression is responsible for the behavior of  $\overline{\mathcal{F}}$  shown in Fig. 2 of the main text.

In Fig. 8 we show Eqs. (C2) and (C3) at  $T = 0$ , and in Fig. 9 we show Eqs. (C2) and (C3) at  $T > 0$  as a function of the tuning parameter  $\Delta$ . Looking at both Figs. 8 and 9, we realize that before the first QCP,  $\Delta = -1$ , the overall maximum fidelity  $\overline{\mathcal{F}}$  is given by  $\overline{F}(S_{\phi^\mp})$ . Between the two QCPs we have either  $\overline{F}(S_{\phi^\mp})$  or  $\overline{F}(S_{\psi^\mp})$  as the maximum


 FIG. 10.  $\langle \overline{F}(S_k) \rangle$  as a function of  $\Delta$  at the absolute zero temperature.

FIG. 11. Same as Fig. 10 but at  $kT = 1.0$ .

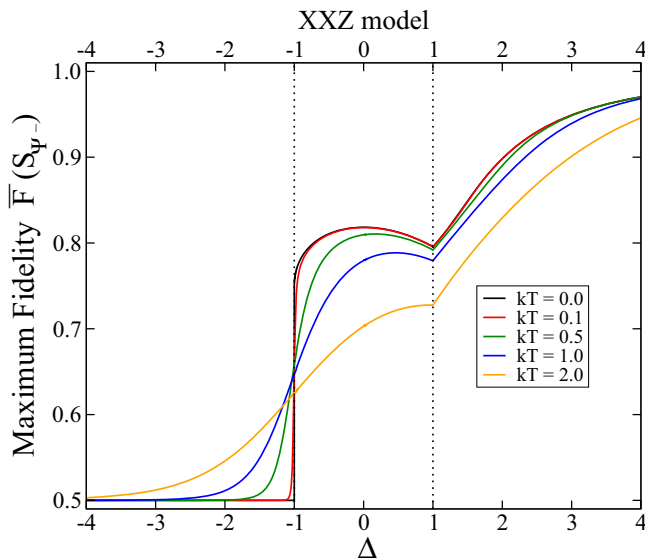
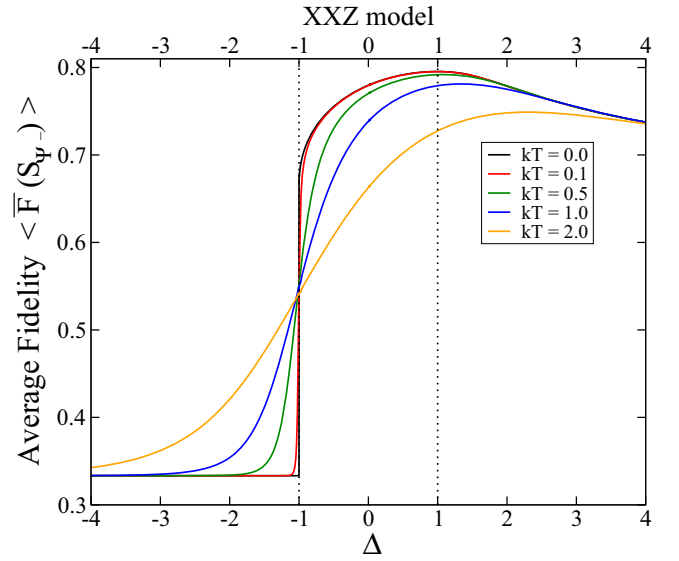
fidelity. And after the second QCP,  $\Delta = 1$ , it is  $\bar{F}(S_{\Psi_+})$  that dominates. The change of which  $\bar{F}(S_k)$  dominates at the QCPs is the reason for the cusplike behavior of  $\bar{F}$ .

A similar analysis allows us to understand the behavior of the maximum average fidelity  $\langle \bar{F} \rangle$  as shown in Fig. 3 of the main text. We now investigate  $\langle \bar{F}(S_k) \rangle$ , Eq. (13) of the main text, for each one of the four possible values of  $k$ ,

$$\langle \bar{F}(S_{\Psi_+}) \rangle = (3 \mp 2xx - zz)/6, \quad (C4)$$

$$\langle \bar{F}(S_{\Phi_+}) \rangle = (3 + zz)/6. \quad (C5)$$

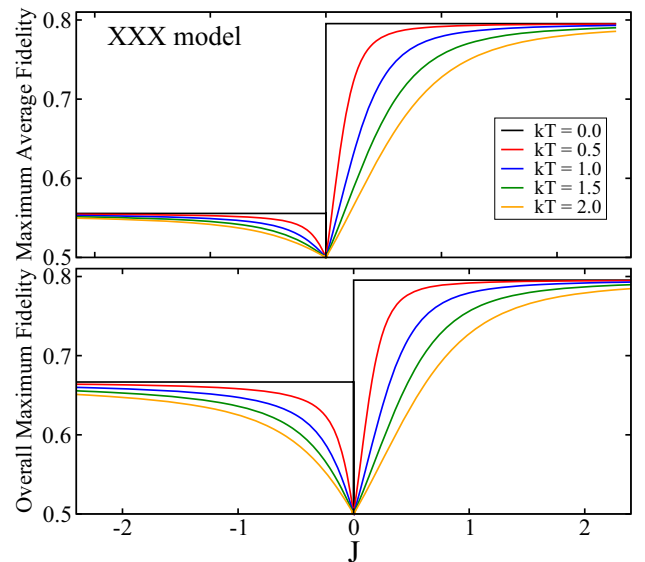
Looking at Figs. 10 and 11, we note that before the first QCP,  $\Delta = -1$ , the maximum average fidelity  $\langle \bar{F} \rangle$  is given by  $\langle \bar{F}(S_{\Phi_+}) \rangle$ . After the first QCP we have  $\langle \bar{F}(S_{\Psi_-}) \rangle$  as the maximum average fidelity. This trend continues even after the second QCP, where  $\langle \bar{F}(S_{\Psi_-}) \rangle$  achieves its maximum. That

FIG. 12.  $\bar{F}(S_{\Psi_-})$  as a function of  $\Delta$  for several values of temperature. Temperatures increase from top to bottom when  $\Delta > -1$ .FIG. 13.  $\langle \bar{F}(S_k) \rangle$  as a function of  $\Delta$  for several values of temperature. Temperatures increase from top to bottom when  $\Delta > -1$ .

is why we do not see any cusplike behavior at  $\Delta = 1$ , the second QCP. At this QCP, there is no change in the function maximizing the average fidelity. Before, at, and after  $\Delta = 1$ , it is always  $\langle \bar{F}(S_{\Psi_-}) \rangle$  that maximizes the average fidelity.

Incidentally, looking at Figs. 10 and 11, we realize that by monitoring both the maximum and the minimum average fidelity, we can detect both QCPs via a cusplike behavior. Indeed, monitoring the maximum average fidelity, we see a cusplike behavior at  $\Delta = -1$ , the first QCP. This is what is shown in Fig. 3 of the main text. However, if we plot the minimum average fidelity,

$$\langle \bar{F} \rangle_{\min} = \min_{\{S_k\}} \langle \bar{F}(S_k) \rangle, \quad (C6)$$

FIG. 14.  $\langle \bar{F} \rangle$  (upper panel) and  $\bar{F}$  (lower panel) for a spin-1/2 chain in the thermodynamic limit. Temperatures increase from top to bottom.



we will see a cusplike behavior not in the first but in the second QCP. At  $\Delta = 1$ , we see that the function giving the minimum average fidelity changes. Before  $\Delta = 1$ , the minimum is achieved by  $\langle \bar{F}(S_{\Psi^+}) \rangle$  and after it the minimum is given by  $\langle \bar{F}(S_{\Phi^+}) \rangle$ . This change of the function minimizing the average fidelity leads to a cusplike behavior at this QCP. As such, by monitoring both the maximum and minimum of  $\langle \bar{F}(S_k) \rangle$ , we can build an input state-independent fidelity as sharp as the state-dependent fidelity in detecting both QCPs, with the advantage that the computation of the former quantity is easily scalable to high spin systems.

We finish this Appendix showing  $\bar{F}(S_{\Psi^-})$  and  $\langle \bar{F}(S_{\Psi^-}) \rangle$  (see Figs. 12 and 13) for several values of  $T$ . Although these quantities are not as good as  $\bar{\mathcal{F}}$ ,  $\langle \bar{\mathcal{F}} \rangle$ , and  $\langle \bar{\mathcal{F}} \rangle_{\min}$  to pinpoint a QCP, we can obtain a lot of information about where the QCPs are located by working with them. We also obtain similar results working with  $\bar{F}(S_k)$  and  $\langle \bar{F}(S_k) \rangle$ , where  $k = \Psi^+, \Phi^\mp$ .

#### APPENDIX D: THE XXX MODEL

The XXX model is given by the following Hamiltonian:

$$H = J \sum_{j=1}^L (\sigma_j^x \sigma_{j+1}^x + \sigma_j^y \sigma_{j+1}^y + \sigma_j^z \sigma_{j+1}^z). \quad (\text{D1})$$

This model is essentially the XXZ model with  $\Delta = 1$ , where we can now change the sign of the whole Hamiltonian by varying the parameter  $J$ . As before, we use periodic boundary conditions. The XXX model has one QCP, located at  $J = 0$ . For  $J < 0$  we have the ferromagnetic phase, and for  $J > 0$  we have the antiferromagnetic one.

In Fig. 14 we show  $\langle \bar{\mathcal{F}} \rangle$  and  $\bar{\mathcal{F}}$  as a function of  $J$  for several values of temperature. It is clear from those figures that both  $\langle \bar{\mathcal{F}} \rangle$  and  $\bar{\mathcal{F}}$  detect the QCP at finite  $T$ , similar to what one obtains computing the thermal quantum discord [11]. Also, for  $kT \gtrsim 0.1$ , the entanglement is already zero before, at, and after the QCP [11].

- 
- [1] S. Sachdev, *Quantum Phase Transitions* (Cambridge University Press, Cambridge, 1999).
- [2] M. Greiner, O. Mandel, T. Esslinger, T. W. Hänsch, and I. Bloch, *Nature (London)* **415**, 39 (2002).
- [3] V. F. Gantmakher and V. T. Dolgoplov, *Phys. Usp.* **53**, 1 (2010).
- [4] S. Rowley, R. Smith, M. Dean, L. Spalek, M. Sutherland, M. Saxena, P. Alireza, C. Ko, C. Liu, E. Pugh *et al.*, *Phys. Status Solidi B* **247**, 469 (2010).
- [5] L.-A. Wu, M. S. Sarandy, and D. A. Lidar, *Phys. Rev. Lett.* **93**, 250404 (2004).
- [6] T. R. de Oliveira, G. Rigolin, M. C. de Oliveira, and E. Miranda, *Phys. Rev. Lett.* **97**, 170401 (2006); T. R. de Oliveira, G. Rigolin, and M. C. de Oliveira, *Phys. Rev. A* **73**, 010305 (2006); T. R. de Oliveira, G. Rigolin, M. C. de Oliveira, and E. Miranda, *ibid.* **77**, 032325(R) (2008).
- [7] R. Dillenschneider, *Phys. Rev. B* **78**, 224413 (2008).
- [8] M. S. Sarandy, *Phys. Rev. A* **80**, 022108 (2009).
- [9] W. K. Wootters, *Phys. Rev. Lett.* **80**, 2245 (1998).
- [10] T. Werlang and G. Rigolin, *Phys. Rev. A* **81**, 044101 (2010).
- [11] T. Werlang, C. Trippa, G. A. P. Ribeiro, and G. Rigolin, *Phys. Rev. Lett.* **105**, 095702 (2010); T. Werlang, G. A. P. Ribeiro, and G. Rigolin, *Phys. Rev. A* **83**, 062334 (2011); *Int. J. Mod. Phys. B* **27**, 1345032 (2013).
- [12] TQD is the QD computed for systems in equilibrium with a thermal reservoir at temperature  $T$ .
- [13] H. Ollivier and W. H. Zurek, *Phys. Rev. Lett.* **88**, 017901 (2001).
- [14] L. Henderson and V. Vedral, *J. Phys. A* **34**, 6899 (2001).
- [15] Y. Huang, *New J. Phys.* **16**, 033027 (2014).
- [16] A. L. Malvezzi, G. Karpat, B. Çakmak, F. F. Fanchini, T. Debarba, and R. O. Vianna, *Phys. Rev. B* **93**, 184428 (2016).
- [17] C. H. Bennett, G. Brassard, C. Crepeau, R. Jozsa, A. Peres, and W. K. Wootters, *Phys. Rev. Lett.* **70**, 1895 (1993).
- [18] Y. Yeo, *Phys. Rev. A* **66**, 062312 (2002).
- [19] R. Fortes and G. Rigolin, *Phys. Rev. A* **96**, 022315 (2017).
- [20] M. Takahashi, *Thermodynamics of One-dimensional Solvable Models* (Cambridge University Press, Cambridge, 1999).
- [21] A. Klümper, *Ann. Phys.* **504**, 540 (1992); *Z. Phys. B* **91**, 507 (1993).
- [22] M. Bortz and F. Göhmann, *Eur. Phys. J. B* **46**, 399 (2005).
- [23] H. E. Boos, J. Damerau, F. Göhmann, A. Klümper, J. Suzuki, and A. Weiße, *J. Stat. Mech.* (2008) P08010.
- [24] C. Trippa, F. Göhmann, and A. Klümper, *Eur. Phys. J. B* **73**, 253 (2010).
- [25] A. Uhlmann, *Rep. Math. Phys.* **9**, 273 (1976).
- [26] R. Fortes and G. Rigolin, *Phys. Rev. A* **92**, 012338 (2015); R. Fortes, *ibid.* **93**, 062330 (2016).
- [27] G. Gordon and G. Rigolin, *Phys. Rev. A* **73**, 042309 (2006); G. Gordon, *ibid.* **73**, 062316 (2006); *Eur. Phys. J. D* **45**, 347 (2007).
- [28] When we refer to Eq. (12) we use the term “mean fidelity,” while we reserve the term “average fidelity” for Eq. (13).
- [29] X. Rong, J. Geng, F. Shi, Y. Liu, K. Xu, W. Ma, F. Kong, Z. Jiang, Y. Wu, and J. Du, *Nat. Commun.* **6**, 8748 (2015).
- [30] C. E. Bradley, J. Randall, M. H. Abobeih, R. C. Berrevoets, M. J. Degen, M. A. Bakker, M. Markham, D. J. Twitchen, and T. H. Taminiau, *Phys. Rev. X* **9**, 031045 (2019).
- [31] T. Xie, Z. Zhao, X. Kong, W. Ma, M. Wang, X. Ye, P. Yu, Z. Yang, S. Xu, P. Wang *et al.*, *Sci. Adv.* **7**, eabg9204 (2021).
- [32] A. Noiri, K. Takeda, T. Nakajima, T. Kobayashi, A. Sammak, G. Scappucci, and S. Tarucha, *Nature (London)* **601**, 338 (2022).
- [33] X. Xue, M. Russ, N. Samkharadze, B. Undseth, A. Sammak, G. Scappucci, and L. M. Vandersypen, *Nature (London)* **601**, 343 (2022).
- [34] M. T. Mądzik, S. Asaad, A. Youssry, B. Joecker, K. M. Rudinger, E. Nielsen, K. C. Young, T. J. Proctor, A. D. Baczewski, A. Laucht *et al.*, *Nature (London)* **601**, 348 (2022).
- [35] T. Xie, Z. Zhao, S. Xu, X. Kong, Z. Yang, M. Wang, Y. Wang, F. Shi, and J. Du, *arXiv:2212.02831*.
- [36] H. T. Quan, Z. Song, X. F. Liu, P. Zanardi, and C. P. Sun, *Phys. Rev. Lett.* **96**, 140604 (2006).

- [37] P. Zanardi and N. Paunković, *Phys. Rev. E* **74**, 031123 (2006).
- [38] P. Buonsante and A. Vezzani, *Phys. Rev. Lett.* **98**, 110601 (2007).
- [39] W.-L. You, Y.-W. Li, and S.-J. Gu, *Phys. Rev. E* **76**, 022101 (2007).
- [40] S.-J. Gu, H.-M. Kwok, W.-Q. Ning, and H.-Q. Lin, *Phys. Rev. B* **77**, 245109 (2008).
- [41] S.-J. Gu, *Int. J. Mod. Phys. B* **24**, 4371 (2010).
- [42] P. N. Timonin, *J. Exp. Theor. Phys.* **113**, 251 (2011).
- [43] O. Rojas, J. Strečka, O. Derzhko, and S. M. de Souza, *J. Phys.: Condens. Matter* **32**, 035804 (2020).
- [44] M. A. Nielsen and I. L. Chuang, *Quantum Computation and Quantum Information* (Cambridge University Press, Cambridge, 2000).
- [45] We have  $N$  complex coefficients leading to  $2N$  real parameters. However, since an overall phase is irrelevant and we must satisfy the normalization constraint, we are left with  $2N - 2$  independent parameters.